

We are IntechOpen, the world's leading publisher of Open Access books Built by scientists, for scientists

4,800

Open access books available

122,000

International authors and editors

135M

Downloads

Our authors are among the

154

Countries delivered to

TOP 1%

most cited scientists

12.2%

Contributors from top 500 universities



WEB OF SCIENCE™

Selection of our books indexed in the Book Citation Index
in Web of Science™ Core Collection (BKCI)

Interested in publishing with us?
Contact book.department@intechopen.com

Numbers displayed above are based on latest data collected.
For more information visit www.intechopen.com



Behavior of Ionic Liquids Under Nanoconfinement Greatly Affects Actual Friction

Toshio Kamijo, Hiroyuki Arafune, Takashi Morinaga,
Takaya Sato and Kazue Kurihara

Additional information is available at the end of the chapter

<http://dx.doi.org/10.5772/65758>

Abstract

Ionic liquids (ILs) are organic salts consisting of anions and cations that exist as liquids at room temperature. ILs exhibit many attractive properties such as negligible volatility, low flammability, and relatively high thermal stability. These properties can be varied in a controlled fashion through systematic changes in the molecular structure of their constituent ions. Some recent studies have aimed to use ILs as new lubricant materials. However, the behavior of ILs as lubricants on the sliding interfaces has not been elucidated. In this chapter, we describe the nano- and macrolubrication properties of some ILs with different types of anions using resonance shear measurement (RSM) and conventional ball-on-plate-type tribotests, respectively. This study reveals that the properties observed by RSM for nanoscale systems can provide important insights for the study of the friction coefficients (macrolubrication properties) obtained by tribotests.

Keywords: tribology, lubricant, nanolubrication, confinement, friction coefficient

1. Introduction

Ionic liquids (ILs) are expected to be promising candidate materials for new lubricants [1–5]. In particular, their stability under severe conditions, such as ultrahigh vacuum [6, 7] and high temperatures [8], has attracted increasing interest. To choose ILs suitable for use as lubricants, it is important to understand the characteristics of the target materials. However, currently, the details of the lubrication mechanism of ILs are not clearly understood.

The tribological properties of ILs have been studied using a macroscopic tribotester. Most previous research has focused on the lubricating behavior of ILs in the boundary lubrication

regime at high loads of several GPa and on their tribochemical reactions with solid surfaces [9–13]. The formation of tribochemical layers on metal surfaces from ILs containing a halogen such as fluorine under sliding conditions has been studied by X-ray photoelectron spectroscopy (XPS) [9–12], scanning electron microscope with energy dispersive X-ray spectroscopy (SEM-EDS) [9–11], and time-of-flight secondary ion mass spectrometry (TOF-SIMS) [12]. Therefore, ILs have also been used as additives for the formation of a tribochemical layer under high loads of several GPa [14–16]. When used, these layers have been considered to contribute to the reduction of friction in the system.

On the other hand, due to the interest in applying ILs as lubricants, the properties of ILs confined in a nanoscale space have also been studied by atomic force microscopy (AFM) [17–19] and the surface force apparatus (SFA) [20, 21]. The oscillating forces observed by both AFM and SFA demonstrated the layered structure of ILs in narrow gaps. However, the relationship between these nanoscale properties and the macrolubrication properties is still not fully understood even for the same surface and ILs. Motivated by this problem, we have recently used resonance shear measurement (RSM) to show that some ILs form a layered structure in the nanoscale space created by the sliding surface [21, 22]. We also revealed that a nanostructure consisting of only several IL layers had a large influence on macroscale friction.

In this chapter, we describe the nano- and macrolubrication properties of some ILs (**Table 1**) with different anions by using RSM and a conventional ball-on-plate-type tribotester, respectively. This study reveals that ILs with different structures form different nanolayered structures and that their nanoscale behaviors are correlated with their macroscale tribology. In addition to providing information related to the lubrication mechanism of ILs, we also describe the principles for choosing an IL as a lubricant.

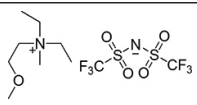
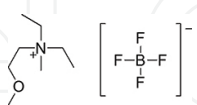
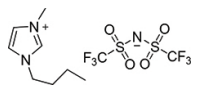
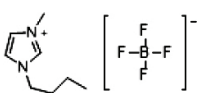
Ionic liquid	Abbreviation	Structure	MW/g	$\rho/\text{g cm}^{-3}$	MV/nm ³	D_m/nm	Viscosity/ mPa s
<i>N,N</i> -diethyl- <i>N</i> -methyl- <i>N</i> -(2-methoxyethyl) ammonium bis (trifluoromethane sulfonyl) imide	[DEME][TFSI]		426.40	1.42	0.49	0.79	77 [22]
<i>N,N</i> -diethyl- <i>N</i> -methyl- <i>N</i> -(2-methoxyethyl) ammonium tetrafluoroborate	[DEME][BF ₄]		233.06	1.17	0.33	0.69	400 [22]
1-Butyl-3-methylimidazolium bis(trifluoromethyl sulfonyl) imide	[BMIM][TFSI]		419.36	1.44	0.48	0.78	58.4 [21]
1-Butyl-3-methylimidazolium tetrafluoroborate	[BMIM][BF ₄]		226.02	1.20	0.31	0.68	124.6 [21]

Table 1. Name, abbreviation, structure, molecular weight (MW), density (ρ), molecular volume (MV), ion pair diameter (D_m), and viscosity (η) of ILs. D_m is determined from (ρ) assuming a cubic packing geometry according to the method described by Horn et al. [23].

2. Nanolubrication properties

2.1. RSM for nanoscale properties of ILs

RSM was performed using an in-house resonance shear system based on an SFA [22], as shown schematically in **Figure 1**. The experimental setup and procedures for RSM are described in detail in a previous publication [21]. Silica sheets used as samples were prepared following the procedure reported by Horn et al. [24]. The root mean square (RMS) roughness value measured by AFM (Toyo Corporation, Agilent 5100 AFM/SPM Microscope) over an area of $5 \times 5 \mu\text{m}^2$ for the silica sheets was 0.31 nm. Using RSM, the resonance curve between the molecularly smooth silica sheets was measured across IL films at a surface separation D with a resolution of 0.1 nm. The value of D was determined from the fringes of equal chromatic order (FECO) analysis. In brief, two back-silvered silica sheets (thickness of ca. 2–4 μm) were glued onto cylindrical quartz lenses (with a radius of curvature (R) of ca. 20 mm) and mounted onto the RSM system. The RSM system was composed of the upper surface unit suspended by a pair of vertical leaf springs and the lower surface unit mounted on a horizontal leaf spring. The upper surface unit was connected to a four-section piezo tube. In this case, it can be laterally oscillated at various frequencies (ω) by an application of a sinusoidal input voltage (U_{in}). The deflection (Δx) of the leaf spring was detected as an output voltage (U_{out}) by a capacitance probe (Microsense 4830, Japan ADE Ltd.). Then, resonance curves were recorded at various D values as the normalized amplitude ($U_{\text{out}}/U_{\text{in}}$) as a function of the frequency ω . RSM was conducted at room temperature (295 ± 0.5 K) and at a humidity of less than 25% maintained by placing silica gel in the sample chamber.

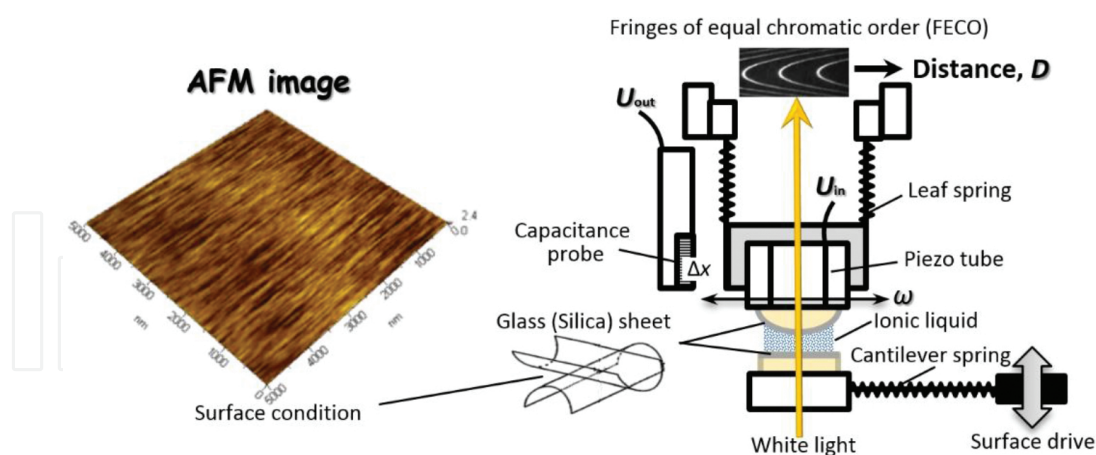


Figure 1. Schematic of the RSM system. The surfaces are in the crossed-cylinder geometry.

The RSM system measured the surface force and resonance shear response by continuously changing the thickness of the liquid film confined between two solid surfaces with a nanometer resolution. The liquid thickness was controlled and determined using interferometric methods in the surface force apparatus. The shear response via resonance method provided a sensitive method for detecting the tiny changes in the liquid properties between the substrates, allowing

us to evaluate the viscosity change associated with liquid structuring, frictional/lubricational property, as well as other properties, by simply changing the liquid film thickness.

Figure 2 shows the typical resonance shear curves for different surface separations. The resonance curves for the two reference states of separation in air (AS) and for silica-silica contact (SC) were measured prior to the RSM of a liquid (**Figure 2**). In the absence of a liquid, the system parameters (mass, damping parameter, and spring constant for the apparatus) determined the AS and SC resonance curves. In the presence of a liquid, the resonance curve at long distances showed a peak at a low frequency that was almost the same as the AS peak. The peak intensity $U_{\text{out}}/U_{\text{in}}$ was lower than the AS peak intensity, corresponding to the energy dissipation due to the bulk viscosity of the liquid. With decreasing D value, the amplitude of the resonance peaks first decreased, and then, the peak disappeared with a further decrease in the distance. For a further decrease in the surface separation, broad resonance curves were observed at intermediate frequencies between the AS and SC frequencies, and the peak frequencies started to shift toward the SC peak because of the weak coupling of the upper and lower surfaces mediated by the confined liquid [25]. When the applied load (N) was further increased by decreasing the surface separation, the peak frequency shifted further toward the SC peak and the amplitude increased, until finally, for a surface separation of 0 nm, the amplitude was almost identical to that of the SC peak. This means that the liquid was completely removed from the gap between the silica surfaces [26]. Similarly, when the applied load (N) was further increased while the surface separation was fixed at a certain distance, the peak frequency also shifted further toward the SC peak frequency, while the amplitude increased. This means that the liquid remained between the silica surfaces at a certain surface separation due to the stronger coupling of the upper and lower surfaces with the increasing applied load.

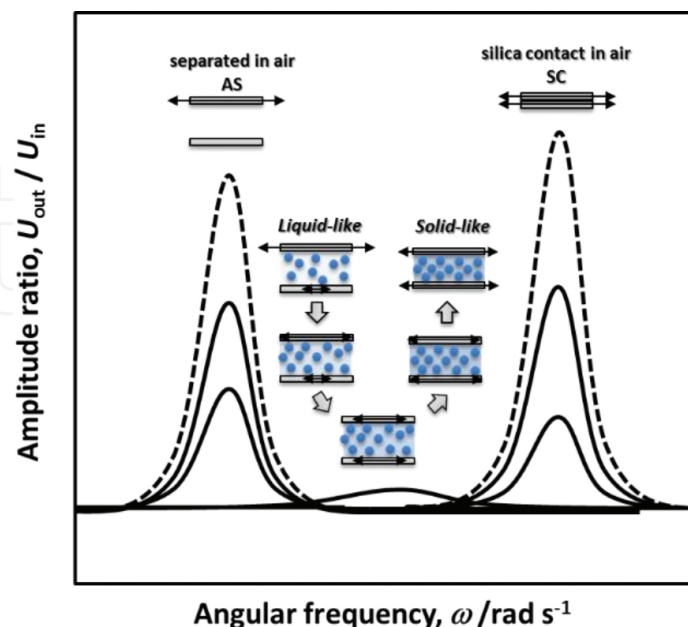


Figure 2. Typical resonance shear curves with different surface separations.

The RSM system described above was used to study the nanolubrication properties of ILs between smooth silica surfaces. **Figure 3(a)** and **(b)** shows the resonance curves for [DEME][TFSI] and [DEME][BF₄] ILs confined between silica surfaces at various separation distances. For reference, the resonance curves for AS and SC were measured prior to the resonance shear measurement of the ILs (**Figure 3**). In the absence of the ILs, the system parameters (mass, damping parameter, and spring constant for the apparatus) determined the AS and SC resonance curves. In the presence of [DEME][TFSI], the resonance curve at $D = 228.1$ nm showed a peak at a frequency of 185 rad s^{-1} that was almost the same as the AS peak. The peak intensity $U_{\text{out}}/U_{\text{in}}$ was lower than the AS peak intensity, corresponding to the energy dissipation due to the bulk viscosity of the IL. With decreasing D value, the amplitude of the resonance peaks started to decrease at 10.2 nm and disappeared at $D = 4.9$ nm. In the range from $D = 4.9$ to 2.5 nm, broad resonance curves were observed at intermediate frequencies between the AS and SC frequencies, and the peak frequency started to shift toward the SC peak because of the weak coupling of the upper and lower surfaces mediated by the confined [DEME][TFSI] [21]. When the applied load (N) was increased further, the surface separation did not change and remained at 2.5 nm (**Figure 4**); however, the peak frequency shifted further toward that of the SC peak and the amplitude increased. This means that [DEME][TFSI] remained between the silica surfaces at the separation of 2.5 nm, and the coupling of the upper and lower surfaces became stronger with the increased applied load.

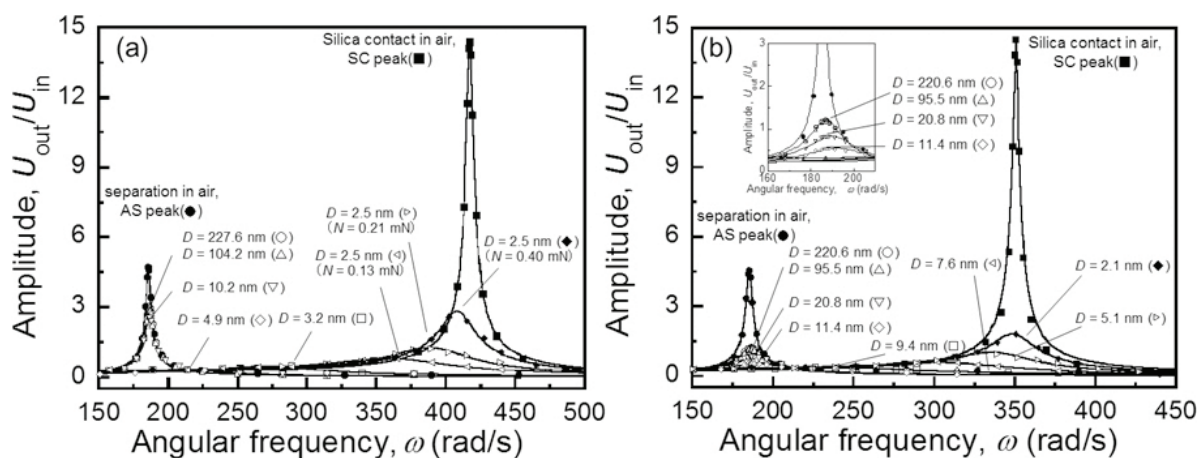


Figure 3. Resonance curves for (a) [DEME][TFSI] and (b) [DEME][BF₄] confined between the silica surfaces at various separation distances under an applied load N . Resonance curves for AS and SC are also shown [22]. Solid lines denote the best fit curves to a physical model [27].

The resonance shear behavior of [DEME][BF₄] (**Figure 3(a)**) was similar to that of [DEME][TFSI], except in the small D region below 2.5 nm (**Figure 3(b)**). The resonance curves at 186 rad s^{-1} did not change in the D range from 220.6 to 95.5 nm, and their amplitudes started to decrease at $D = 20.8$ nm. The resonance frequencies of these curves were almost the same as the frequency of the AS peak. The amplitude of the resonance peaks gradually decreased with decreasing D from 20.8 to 11.4 nm and disappeared at $D = 9.4$ nm. This distance is higher than the disappearance distance ($D = 4.9$ nm) for [DEME][TFSI]. In the range from $D = 9.4$ to 2.1 nm, broad resonance curves were observed at intermediate frequencies, and the peak

frequencies started to shift toward the frequency of the SC peak because of the weak coupling of the upper and lower surfaces mediated by the confined [DEME][BF₄]. When the applied load (N) was further increased, the surface separation remained at 2.1 nm (**Figure 4**), indicating that [DEME][BF₄] remained trapped between the silica surfaces.

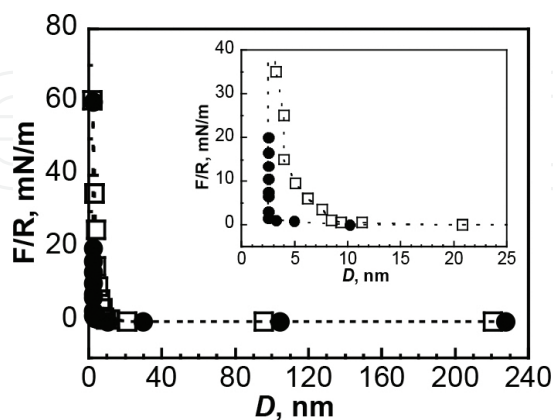


Figure 4. Profiles of normal force normalized by surface curvature radius (F/R) as a function of surface separation D between silica surfaces in [DEME][TFSI] (●) and [DEME][BF₄] (□) [22].

2.2. Dynamics of ILs by changing the load applied to the two friction surfaces

Figure 5 plots the relative intensity (I_r) of the resonance peak, that is, the ratio of the peak intensity for confined ILs is divided by the SC peak intensity as a function of applied load. This intensity ratio is a measure of the lubrication behavior of the confined ILs, with smaller values indicating better lubrication behavior. With an increase in the applied load from 0.21 to 0.33 mN, the I_r values of [DEME][TFSI] clearly increased from ca. 0.09 to 0.16 and then plateaued when the load was increased to 0.40 mN. The I_r of [DEME][BF₄] showed a behavior similar to that of [DEME][TFSI], gradually increasing from ca. 0.07 to 0.12 as the applied load increased from 0.19 to 0.50 mN, and reaching a plateau when the load was increased to 0.70 mN. The noteworthy difference between the two ILs was observed at higher loads (>0.4 mN), with the 0.18 I_r value obtained for [DEME][TFSI] being significantly larger than the 0.12 value obtained for [DEME][BF₄]. These results indicate that, under higher loads (>0.4 mN), [DEME][BF₄] is a better lubricant than [DEME][TFSI]. Additionally, RSM revealed that an IL layer with ca. 2 nm thickness was maintained between the silica surfaces even under high applied loads (>0.4 mN). The plateau of the relative intensity under applied loads (>0.4 mN) indicated that the IL layer confined between the silica surfaces maintained its lubricating properties.

2.3. Effective viscosity (η_{eff}) of the confined ILs measured to quantitatively measure lubrication performance

We analyzed the resonance curves using a previously developed physical model [27] to obtain a quantitative understanding of the properties of the confined ILs. The details of the analytical procedure are described in the literature [21, 27]. **Figure 6** plots the effective viscosity (η_{eff}) obtained for the ILs using the model versus the separation distance between the silica surfa-

ces. The η_{eff} values at larger separations were constant and essentially identical to the bulk IL viscosity of 400 for [DEME][BF₄] and 77 mPa s for [DEME][TFSI]. However, the η_{eff} value increased sharply with decreasing D below 11.4 nm for [DEME][TFSI] and below 10.4 nm for [DEME][BF₄]. The η_{eff} value for [DEME][TFSI] confined in the nanospace ($D \leq 4.9$ nm) was one to two orders of magnitude higher than that at larger separations ($D \geq 10.2$), and the η_{eff} value for [DEME][BF₄] confined in the nanospace ($D \leq 9.4$ nm) was about one order of magnitude higher than that at larger separations ($D \geq 11.4$). Note that in the nanospace, the η_{eff} value of [DEME][TFSI] was higher than that of [DEME][BF₄], whereas in the bulk, the opposite was the case and the viscosity of [DEME][BF₄] was higher than that of [DEME][TFSI]. This behavior is similar to the trend shown by the ILs [BMIM][TFSI] and [BMIM][BF₄] confined between the silica surfaces [21], even though the cations used in this study are different from those used in Ref. [21].

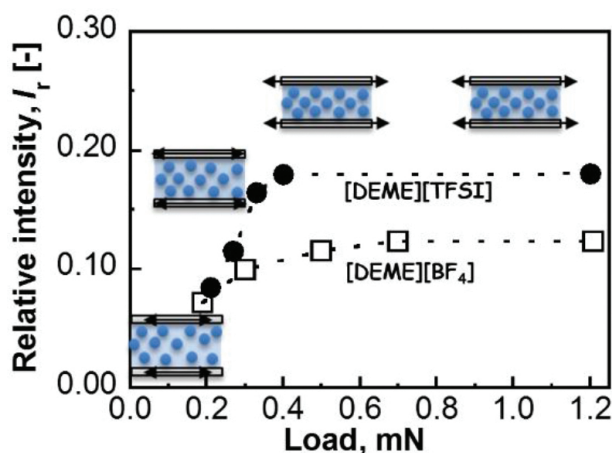


Figure 5. Relative intensity (peak intensity confined ILs/SC peak intensity) versus the applied load for [DEME][TFSI] (●) and [DEME][BF₄] (□) [22].

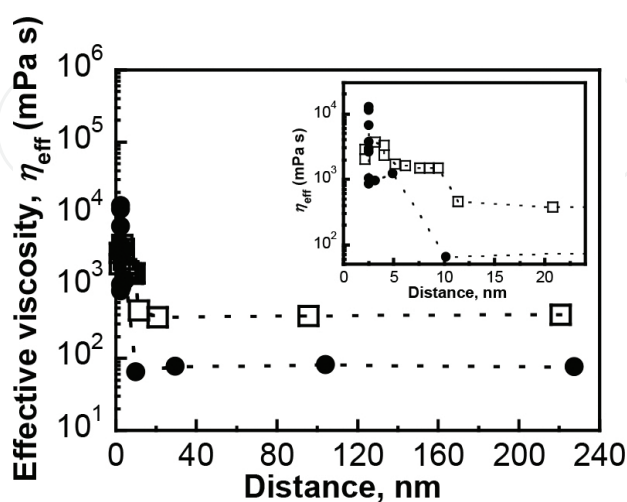


Figure 6. Effective viscosity η_{eff} versus the separation distance for [DEME][TFSI] (●) and [DEME][BF₄] (□) [22].

We suppose that the rapid increase in the effective viscosity with decreasing distance observed in **Figure 6** corresponds to the distance at which the formation of a solid-like structure due to the confinement is initiated. For [DEME][BF₄], the sharp viscosity increase began at a clearly shorter distance than that for [DEME][TFSI], indicating that this ammonium salt restructures more readily than the TFSI salt, or in other words, that the BF₄ salt is more easily crystallized. This consideration is also supported by the results of the crystallization temperature measurement using differential thermal calorimetry (DSC) [28]. As indicated by the DSC measurements, [DEME][BF₄], for which the viscosity increases at a relatively long distance, shows a distinct crystallization temperature, whereas the TFSI salt only shows a glass transition temperature but not a crystallization temperature. The same trend is found for aromatic ILs. The viscosity of [BMIM][TFSI], which has a specific crystallization temperature, rises rapidly at a large distance, whereas the viscosity of [BMIM][BF₄], which does not show a crystallization temperature, rises rapidly only at a short distance [29].

Figure 7 plots η_{eff} versus the applied load. The η_{eff} values for [DEME][TFSI] and [DEME][BF₄] increased with the applied load and plateaued when the load was increased to 0.4 mN. At higher loads (>0.4 mN), η_{eff} of ca. 13,000 for [DEME][TFSI] was larger than the ca. 3000 value obtained for [DEME][BF₄].

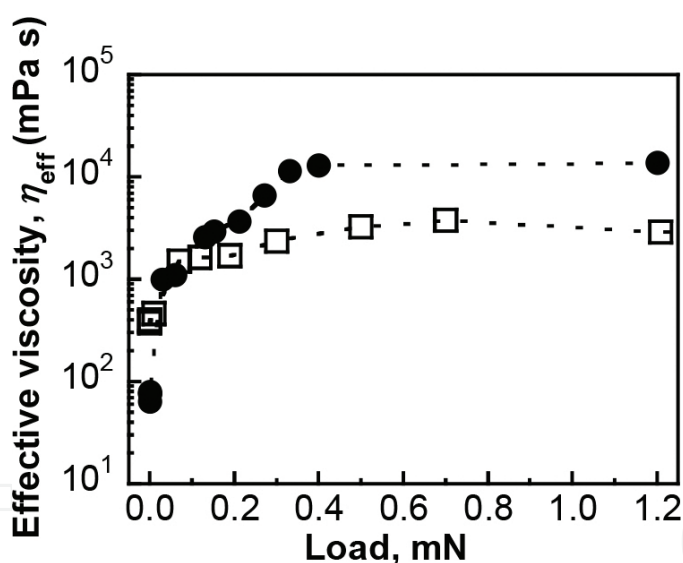


Figure 7. Plots of the effective viscosity η_{eff} versus the applied load for [DEME][TFSI] (●) and [DEME][BF₄] (□) [22].

In the RSM, the facing silica surfaces were completely separated to avoid partial contact and to allow the analysis of the boundary lubrication property of the confined liquid at a certain separation distance. In this configuration, an increase in the viscosity of the lubricant layer under confinement directly leads to increased friction at the sliding interface. The results obtained from RSM showed that the η_{eff} of [DEME][BF₄] is lower than that of [DEME][TFSI] at a similar separation distance (ca. 2 nm), meaning that under such confinement, the lubrication performance of [DEME][BF₄] is better than that of [DEME][TFSI]. We thus concluded that, for higher loads (>0.4 mN), [DEME][BF₄] is a better lubricant than [DEME][TFSI].

3. Macroscopic tribological properties

3.1. Reciprocating-type tribotests for evaluation of macroscopic properties

Friction measurements were carried out using a conventional reciprocating tribotester, TRIBOGEAR TYPE 38 (Shinto Scientific Co. Ltd., Tokyo), using a glass ball of 10 mm ϕ and a glass plate. To obtain a clean surface, the glass ball and glass plate were treated in fresh nitric acid at 373 K for 75 min. The RMS roughness values measured by AFM for the glass ball and plate were 9.9 and 1.2 nm over an area of 5 \times 5 μ m², respectively. A schematic of the tribotester is shown in **Figure 8**. The measurements were performed at a movement distance of 10 mm, with a sliding velocity ranging from 5.0 \times 10⁻⁴ to 3.0 \times 10⁻² m s⁻¹ under an applied load of 196–980 mN at room temperature (295 \pm 0.5 K). The friction force was measured by an all-in-one load converter from a gauge attached to the sample holder and was recorded as a function of time. The friction coefficient (μ) was calculated as the friction force divided by the normal load. Friction coefficients obtained for at least five trials were recorded and averaged.

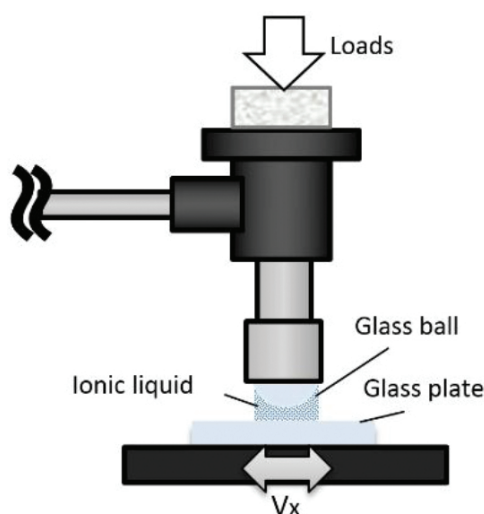


Figure 8. Schematic of reciprocating-type tribotester.

The Stribeck diagram of the friction behavior is used to explain the rubbing phenomena occurring in lubricated contacts [30]. A schematic representation of the Stribeck diagram is shown in **Figure 9**. For high values of $\eta V/N$, the friction coefficient is linearly ascending due to fluid film lubrication, and the friction is related to the viscous dragging forces in the fluid film. When the load increases or fluid viscosity and/or velocity decreases, the $\eta V/N$ factor falls. Then, the fluid film becomes thinner, and consequently, the friction coefficient decreases down to the minimum value. For even smaller $\eta V/N$ values, the fluid film thickness is further reduced and solid-to-solid contact starts to occur, leading to an increase in the friction coefficient as the $\eta V/N$ factor decreases. Such a rise in the friction coefficient is also related to the fluid viscosity increase in some regions of the contact area under high contact pressure. These phenomena characterize the mixed lubrication regime. Further reduction in the $\eta V/N$ factor strengthens

the solid-to-solid contact, and the film thickness becomes smaller than the height of the surface asperities, leading to the transition of the boundary lubrication regime.

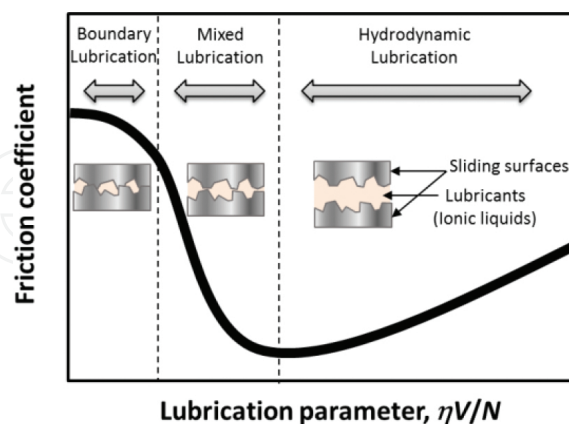


Figure 9. Schematic of Stribeck diagram; friction coefficient as a function of the lubrication parameter: $\eta V/N$. η : fluid viscosity, V : sliding velocity, N : normal load.

We studied the boundary lubrication properties of ILs between a glass ball and a glass plate by using a macroscopic tribotester. **Figure 10** plots the friction coefficients between a glass ball and a glass plate in [DEME][TFSI] or [DEME][BF₄] versus the sliding velocity (V) divided by the load (L) ($\text{m s}^{-1} \text{N}^{-1}$). The measurements were conducted by sliding a glass plate over a distance of 10 mm at various sliding velocities from 5.0×10^{-4} to $3.0 \times 10^{-2} \text{ m s}^{-1}$ and under various applied loads from 196 to 980 mN at 298 K. The friction coefficient for [DEME][BF₄] increased from 0.05 to 0.08 as the V/L parameter decreased from 1.5×10^{-1} to 5.1×10^{-3} and was nearly constant at $\mu \approx 0.08$ over the V/L range of 5.1×10^{-3} to 1.0×10^{-3} . The friction coefficient results for [DEME][TFSI] were similar to those for [DEME][BF₄]; however, the friction coefficient observed in the region of V/L ranging from 1.5×10^{-1} to 1.0×10^{-4} was significantly higher than that of [DEME][BF₄]. Such dependence of the friction coefficient on V/L corresponds to the shift in the lubrication regime of [DEME][TFSI] and [DEME][BF₄] from mixed lubrication to boundary lubrication. As a control, the friction coefficient was measured between the glass ball and glass plate without an IL and was found to be ≈ 0.7 at the sliding velocity of $1.0 \times 10^{-3} \text{ m s}^{-1}$ and under a normal load of 196 mN. Thus, the presence of ILs at the glass-glass interface dramatically reduced the friction coefficient to less than 20% of the value obtained without ILs.

3.2. Comparison of measurement results revealing a correlation between the macroscale friction phenomena and the physicochemical properties of ILs in nanospace

For a confined IL, boundary lubrication is dominant, and the contribution of hydrodynamic lubrication due to the change in lubricant thickness is not effective. Therefore, the difference in boundary lubrication under the measurement conditions between [DEME][BF₄] and [DEME][TFSI] can be explained based on the effective viscosity obtained from RSM. The obtained RSM results showed that the η_{eff} of [DEME][BF₄] was lower than that of [DEME][TFSI] when these ILs were maintained at a similar separation distance (ca. 2 nm), indicating that the

lubrication performance of [DEME][BF₄] is better than that of [DEME][TFSI] under such confined conditions. The inversion of the order of IL viscosities under confinement from the order of bulk viscosity values appears to be due to the differences in the layering structure of the ILs due to the differences in their anion structure.

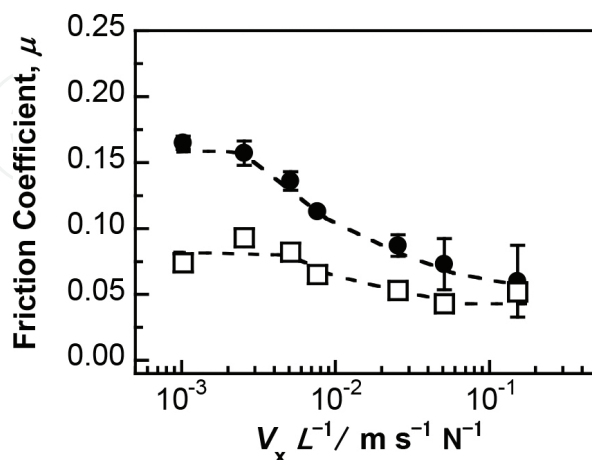


Figure 10. Friction coefficient between a glass ball and a glass plate in [DEME][TFSI] (●), in [DEME][BF₄] (□), by sliding the glass plate over a distance range of 10 mm at sliding velocity of $5.0 \times 10^{-4} \text{ m s}^{-1}$ – $3.0 \times 10^{-2} \text{ m s}^{-1}$ and under an applied load of 196–980 mN at 298 K. Dashed lines are guides to the eyes [22].

We now discuss the possible structural origin for the observed viscosity effects. Canova et al. studied the layering structure of ILs ([BMIM][TFSI] and [BMIM][BF₄]) confined to a silica contact plane using molecular dynamics simulations. For [BMIM][TFSI], it was found that ion pairs orient alternately to form a checker-board structure. This means that each ion is forced to contact ions with the same charge during shearing [31]. The repulsive force between the ions with the same sign of the charge destabilizes the crystal structure of the IL and triggers an overall restructuring of inner molecular layers to form a more stable configuration, resulting in high friction. In contrast, [BMIM][BF₄] formed a layer-by-layer structure where cations and anions did not suffer from such repulsions because each ion layer is sandwiched between the oppositely charged layers, leading to smooth shearing and low friction. Even though the cations used in our study are different from those studied by Canova et al., based on this insight, we ascribe the better boundary lubrication performance of [DEME][BF₄] relative to that of [DEME][TFSI] to the differences in the layered structures of these ILs under confinement.

The RSM showed that ILs were maintained between the silica surfaces at a surface separation of 2.5 nm for [DEME][TFSI] and 2.1 nm for [DEME][BF₄], which are usually referred to as hard-wall thicknesses. Assuming a cubic packing geometry and following Horn et al.'s [23] method, the diameters of the ion pairs determined from the density were 0.79 nm for [DEME][TFSI] and 0.69 nm for [DEME][BF₄]. Based on these values, we determined that in both systems, three layers of ILs were trapped between the silica surfaces. The dramatic reduction in the friction coefficient in “the boundary lubrication region” with ILs was presumably due to the presence of the three layers of ILs between the silica surfaces under an applied load of 196 mN.

These results indicated that the tribotester macroscopic tribological properties correspond to the nanoscale lubrication properties obtained from nanoscopic RSM.

4. Conclusion

We performed RSM and reciprocating-type tribotests to evaluate the friction properties of lubrication systems consisting of some types of ILs between the silica surfaces. In the case of [DEME][BF₄] and [DEME][TFSI], the RSM results revealed that IL layers with a thickness of ca. 2 nm remained between the silica surfaces under applied loads. For these conditions, the effective viscosity of the IL including BF₄ anion was smaller than that of the IL including the TFSI anion. Similarly, in the boundary lubrication regime, the friction coefficient μ of [DEME][BF₄] obtained by the tribotests was lower than that of [DEME][TFSI]. Even though the RSM and tribotest measurement were performed under different applied loads, the difference in the friction coefficient between [DEME][TFSI] and [DEME][BF₄] in the boundary lubrication regime observed by the tribotest corresponded to their behavior under confinement between the silica surfaces, as observed by RSM. These results indicate that the nanoscale properties observed by RSM can provide important insights for the study of the friction coefficients (macrolubrication properties) obtained by the tribotests.

Acknowledgements

This work was supported in part by the “Green Tribology Innovation Network” Advanced Environmental Materials Area, Green Networks of Excellence (GRENE) program and Grants-in-Aid for Scientific Research (nos. 25810091, 26820034, and 30399258) sponsored by the Ministry of Education, Culture, Sports, Science and Technology (MEXT) in Japan.

Author details

Toshio Kamijo¹, Hiroyuki Arafune¹, Takashi Morinaga¹, Takaya Sato^{1*} and Kazue Kurihara^{2,3}

*Address all correspondence to: takayasa@tsuruoka-nct.ac.jp

1 Department of Creative Engineering, National Institute of Technology, Tsuruoka College, Tsuruoka, Japan

2 Institute of Multidisciplinary Research for Advanced Materials (IMRAM), Tohoku University, Aoba-ku, Sendai, Japan

3 WPI-Advanced Institute of Materials Research (WPI-AIMR), Tohoku University, Aoba-ku, Sendai, Japan

References

- [1] Ye C, Liu W, Chen Y, Yu L. Room-temperature ionic liquids: a novel versatile lubricant. *Chem. Commun.* 2001;21:2244–2245. DOI: 10.1039/b106935g
- [2] Minami I. Ionic liquids in tribology. *Molecules* 2009;14:2286–2305. DOI: 10.3390/molecules14062286
- [3] Zhou F, Liang Y, Liu W. Ionic liquid lubricants: designed chemistry for engineering applications. *Chem. Soc. Rev.* 2009;38:2590–2599. DOI: 10.1039/b817899m
- [4] Kondo H. Tribochemistry of ionic liquid lubricant on magnetic media. *Adv. Tribol.* 2012;2012:1–20. DOI: 10.1155/2012/526726
- [5] Somers A, Howlett P, MacFarlane D, Forsyth M. A review of ionic liquid lubricants. *Lubricants* 2013;1:3–21. DOI: 10.3390/lubricants1010003
- [6] Suzuki A, Shinka Y, Masuko M. Tribological characteristics of imidazolium-based room temperature ionic liquids under high vacuum. *Tribol. Lett.* 2007;27:307–313. DOI: 10.1007/s11249-007-9235-8
- [7] Street KW, Morales W, Koch VR, Valco DJ, Richard RM, Hanks N. Evaluation of vapor pressure and ultra-high vacuum tribological properties of ionic liquids. *Tribol. Trans.* 2011;54:911–919. DOI: 10.1080/10402004.2011.606963
- [8] Phillips BS, John G, Zabinski JS. Surface chemistry of fluorine containing ionic liquids on steel substrates at elevated temperature using mössbauer spectroscopy. *Tribol. Lett.* 2007;26:85–91. DOI: 10.1007/s11249-006-9020-0
- [9] Lu Q, Wang H, Ye C, Liu W, Xue Q. Room temperature ionic liquid 1-ethyl-3-hexylimidazolium-bis(trifluoromethylsulfonyl)-imide as lubricant for steel–steel contact. *Tribol. Int.* 2004;37:547–552. DOI: 10.1016/j.triboint.2003.12.003
- [10] Jiménez AE, Bermúdez MD, Iglesias P, Carrión FJ, Martínez-Nicolás G. 1-N-alkyl-3-methylimidazolium ionic liquids as neat lubricants and lubricant additives in steel–aluminium contacts. *Wear* 2006;260:766–782. DOI: 10.1016/j.wear.2005.04.016
- [11] Liu X, Zhou F, Liang Y, Liu W. Tribological performance of phosphonium based ionic liquids for an aluminum-on-steel system and opinions on lubrication mechanism. *Wear* 2006;261:1174–1179. DOI: 10.1016/j.wear.2006.03.018
- [12] Kamimura H, Kubo T, Minami I, Mori S. Effect and mechanism of additives for ionic liquids as new lubricants. *Tribol. Int.* 2007;40:620–625. DOI: 10.1016/j.triboint.2005.11.009
- [13] Qu J, Chi M, Meyer HM, Blau PJ, Dai S, Luo H. Nanostructure and composition of tribo-boundary films formed in ionic liquid lubrication. *Tribol. Lett.* 2011;43:205–211. DOI: 10.1007/s11249-011-9800-z

- [14] Qu J, Bansal DG, Yu B, Howe JY, Luo H, Dai S, Li H, Blau PJ, Bunting BG, Mordukhovich G, Smolenski DJ. Antiwear performance and mechanism of an oil-miscible ionic liquid as a lubricant additive. *ACS Appl. Mater. Interfaces* 2012;4:997–1002. DOI: 10.1021/am201646k
- [15] Zhou Y, Dyck J, Graham TW, Luo H, Leonard DN, Qu J. Ionic liquids composed of phosphonium cations and organophosphate, carboxylate, and sulfonate anions as lubricant antiwear additives. *Langmuir* 2014;30:13301–13311. DOI: 10.1039/b817899m
- [16] Lo ER, Reichelt M, Salgado J. Ionic liquids based on phosphonium cations as neat lubricants or lubricant additives for a steel/steel contact. *ACS Appl. Mater. Interfaces* 2014;6:13115–13128. DOI: 10.1021/am502980m
- [17] Hayes R, El Abedin SZ, Atkin R. Structure in confined room-temperature ionic liquids. *J. Phys. Chem. B* 2009;113:7049–7052. DOI: 10.1021/jp902837s
- [18] Atkin R, Warr GG. Pronounced structure in confined aprotic room-temperature ionic liquids. *J. Phys. Chem. C* 2007;111:5162–5168. DOI: 10.1021/jp902837s
- [19] Werzer O, Cranston ED, Warr GG, Atkin R, Rutland MW. Ionic liquid nanotribology: mica–silica interactions in ethylammonium nitrate. *Phys. Chem. Chem. Phys.* 2012;14:5147–5152. DOI: 10.1039/c1cp23134k
- [20] Perkin S, Albrecht T, Klein J. Layering and shear properties of an ionic liquid, 1-ethyl-3-methylimidazolium ethylsulfate, confined to nano-films between mica surfaces. *Phys. Chem. Chem. Phys.* 2010;12:1243–1247. DOI: 10.1039/b920571c
- [21] Ueno K, Kasuya M, Watanabe M, Mizukami M, Kurihara K. Resonance shear measurement of nanoconfined ionic liquids. *Phys. Chem. Chem. Phys.* 2010;12:4066–4071. DOI: 10.1039/b923571j
- [22] Kamijo T, Arafune H, Morinaga T, Honma S, Sato T, Hino M, Mizukami M, Kurihara K. Lubrication properties of ammonium-based ionic liquids confined between silica surfaces using resonance shear measurements. *Langmuir* 2015;31:13265–13270. DOI: 10.1021/acs.langmuir.5b03354
- [23] Horn RG, Evans DF, Ninham BD. Double-layer and solvation forces measured in a molten salt and its mixtures with water. *J. Phys. Chem.* 1988;92:3531–3537. DOI: 10.1021/J100323a042
- [24] Horn RG, Smith DT, Haller W. Surface forces and viscosity of water measured between silica sheets. *Chem. Phys. Lett.* 1989;162:404–408. DOI: 10.1016/0009-2614(89)87066-6
- [25] Dushkin CD, Kurihara K. Nanotribology of thin liquid-crystal films studied by the shear force resonance method. *Colloids Surf. A Physicochem. Eng. Asp.* 1997;129–130:131–139. DOI: 10.1016/S0927-7757(97)00031-9

- [26] Mizukami M, Kusakabe K, Kurihara K. Shear resonance measurement on structuring of liquids confined between mica surfaces. *Prog. Colloid Polym. Sci.* 2004;128:105–108. DOI: 10.1007/b97098
- [27] Mizukami M, Kurihara K. A new physical model for resonance shear measurement of confined liquids between solid surfaces. *Rev. Sci. Instrum.* 2008;79:113705. DOI: 10.1063/1.3012811
- [28] Maru MM, Tanaka DK. Consideration of Stribeck diagram parameters in the investigation on wear and friction behavior in lubricated sliding. *J. Braz. Soc. Mech. Sci. Eng.* 2007;29:55–62. DOI: 10.1590/S1678-58782007000100009
- [29] Sato T., Masuda G., Takagi K. Electrochemical properties of novel ionic liquids for electric double layer capacitor applications. *Electrochim. Acta* 2004;49:3603–3611. DOI: 10.1016/j.electacta.2004.03.030
- [30] Tokuda H., Tsuzuki S., Susan M.A.B.H., Hayamizu K., Watanabe, M. How ionic are room-temperature ionic liquids? An indicator of the physicochemical properties. *J. Phys. Chem. B* 2006;110:19593–19600. DOI: 10.1021/jp064159v
- [31] Canova F. F., Matsubara H., Mizukami M., Kurihara K., Shluger A.L. Shear dynamics of nanoconfined ionic liquids. *Phys. Chem. Chem. Phys.* 2014;16:8247–8256. DOI: 10.1039/c4cp00005f

IntechOpen

